DOI: 10.1002/ejic.200900126

Synthesis and Characterization of Single-Crystalline Lanthanum Fluoride with a Ring-Like Nanostructure

Yang Tian,*[a] Jing Wen,[a] Bin Liu,[a] Ning Sui,[b] Qionghua Jin,[a] and Xiuling Jiao*[b]

Keywords: Molten salt synthesis / Nanostructures / Crystal growth / Lanthanum / Halides

LaF_3 ring-like nanostructures with a diameter of less than 2 μm have been fabricated by a facile, effective, and environmentally friendly molten salt synthesis route in which $NaNO_3$ and KNO_3 (2:1 molar ratio) act as reaction media and the rare-earth nitrate and NaF as precursor. X-ray diffraction, TEM, HR-TEM, energy dispersive X-ray spectroscopy, and photoluminescence spectroscopy are all used to characterize the as-prepared samples. Experiments peformed with different reaction times indicate that a central-etching of the plates from the inner part towards the edge during nanocrystal growth plays a key role in the formation of LaF_3 nanorings since no other templates/surfactants are present in our system. Additionally, the luminescence properties of LaF_3 nanorings doped with Eu^{3+} cation have been investigated and compared with those of bulk materials and nanoparticles with a size of approximately 50 nm.

Introduction

The direct fabrication of complex architectures with controlled morphology and dimensionality is always important because such control is critical in investigating the shape and structural dependence of many applications. Among those various architectures, ring-like building blocks have attracted intense research interest because of their novel properties and promising applications in the design of complex nanostructures for precise nanofabrication.[1] For example, the holes in the nanorings can be used as nanovessels for biomolecular probes and for smaller nanostructures as multifunctional materials.[2] To date, ring-like structures have been obtained by electron beam lithography and hard template-assisted techniques,[3] although the high cost and complexity associated with the templates limits the practical applications of these approaches. In recent years, a few ring-like nanostructures, such as CdS, ZnO, $Cd(OH)_2$, Fe_2O_3, Co, $Ag_2V_4O_{11}$ and so on, have been successfully synthesized by wet chemical methods in aqueous and organic solutions.[4] However, the challenge of developing simple "bottom-up" techniques for the fabrication of ring-like architectures in solvents such as ionic liquids and molten salts still remains.

Molten salts are completely ionized nonaqueous solvents which have a unique and rich chemical character.[5] Changes to the amount and properties of the salts used could have profound effects on crystal growth, which would be reflected in the morphology and physicochemical characteristics of the products formed. Molten salt synthesis has been shown to be a promising route for the preparation of metal-oxide materials, especially for the synthesis of nanomaterials, and many new types of nanomaterials have been prepared by this method.[6,7] However, there have been few reports on the fabrication of ring-like nanostructures in molten salts.[7]

Rare-earth fluorides are a class of materials with great potential in optical applications, such as phosphors in lamps and display devices, components in optical telecommunications, light-emitting diodes (LEDs), biological labelling, and solid-state lasers.[8] The size- and shape-controlled synthesis of rare-earth fluoride nanomaterials has therefore attracted a great deal of attention during the past few years and many methods have been developed for their preparation. For example, Yan and co-workers have prepared single-crystal and monodisperse LaF_3 triangular nanoplates via a $La(CF_3COO)_3$ pyrolysis route,[9] and Li and co-workers have successfully employed hydrothermal routes to yield fullerene-like nanoparticles and Ln^{3+}-doped, bundle-like YF_3 phosphors.[10] Similarly, Cao et al. have obtained CeF_3 nanocrystals in the form of disks, rods, and dots via a mild ultrasound-assisted route from an aqueous solution containing different fluorine sources,[11] and Chen et al. have reported a hydrothermal route for the preparation of hollow peanut-like structures of YF_3 using the tetrafluoroborate complex as the fluoride source.[12] Ritcey et al. have used reverse microemulsions to prepare hexagonal and triangular YF_3 nanocrystals,[13] Yao et al. have successfully prepared YF_3 sub-microsized truncated octahedra with

[a] Department of Chemistry, Capital Normal University, Beijing 100048, P. R. China
Fax: +86-010-68903040
[b] School of Chemistry and Chemical Engineering, Shandong University, Jinan 250100, P. R. China
E-mail: tianyang@mail.sdu.edu.cn
Supporting information for this article is available on the WWW under http://www.eurjic.org or from the author.

Eu^{3+} doping,[14] and Lin and co-workers have prepared lanthanide fluorides with multiform structures and morphologies by hydrothermal synthesis.[15] Different EuF_3-based structures have also been fabricated recently.[16] Despite these advances, the range of rare-earth fluoride geometries still needs to be expanded to meet the increasing nano- and micotechnological demands.

In the present work we report a convenient molten salt method in which a mixture of $NaNO_3$ and KNO_3 (2:1 molar ratio) acts as the reaction medium for the synthesis of hexagonal LaF_3 rings without the need for a surfactant. The high-quality crystalline nature of the LaF_3 structures was confirmed by various analytic techniques and the fluorescent properties of LaF_3 as a host matrix were characterized by doping with Eu^{3+} cation.

Results and Discussion

The sample was investigated by powder X-ray diffraction (XRD) to characterize its phase and crystallization. As shown in Figure 1, all the peaks of XRD pattern are in good agreement with the previously reported hexagonal structure (space group: *P63/mcm*) for crystalline LaF_3 (JCPDS Card 08-0461), with a high degree of crystallinity and few impurities. The crystal cell parameters of the sample were calculated to be $a = 0.7178$ nm and $c = 0.7358$ nm by JADE 5. These calculated values are in agreement with the values given in the JCPDS Card 08-0461 file for LaF_3 ($a = 0.7184$ nm and $c = 0.7351$ nm).

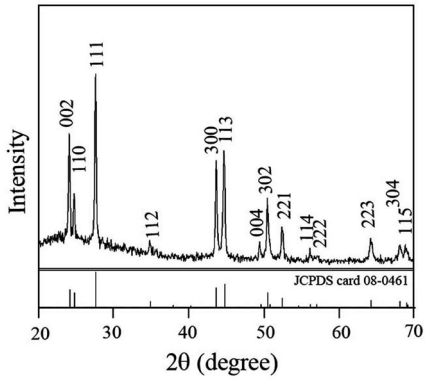

Figure 1. XRD pattern of the as-prepared LaF_3 product.

Figure 2 (a) shows a typical TEM image of the sample. It can be seen that multiple crystals have a ring shape with an almost hexagonal outer-wall and diameters in the range 800–1600 nm. The inset in Figure 2 (a) shows the SEM image, which confirms that the morphology and size are in agreement with those observed by TEM. The inductively coupled plasma mass spectrum (ICP-MS) and the energy dispersive X-ray (EDX) spectrum (Figure S1 in the Supporting Information) of the as-obtained LaF_3 show the expected element signals and stoichiometry, within experimental error. Moreover, the high-resolution TEM (HR-TEM, Figure 2, b) image demonstrates the intrinsic crystallography of the as-obtained LaF_3 nanorings. The lattice fringes on the surface of the nanocrystal (Figure 2, b) show its good crystallization and the fast Fourier transform pattern (FFT, inset in Figure 2, b) shows its single-crystalline nature with a crystallographic orientation [001]. The plane spacing of 0.323 nm corresponds to the (111) and $(1\bar{2}1)$ planes of hexagonal LaF_3, and the plane spacing of 0.360 nm is assigned to the (110) planes. The structure of as-prepared LaF_3 hexagonal nanorings can therefore be indexed with top/bottom surfaces of (001) and side surfaces of {100} and $\{\bar{1}10\}$, as shown schematically in Figure 3.

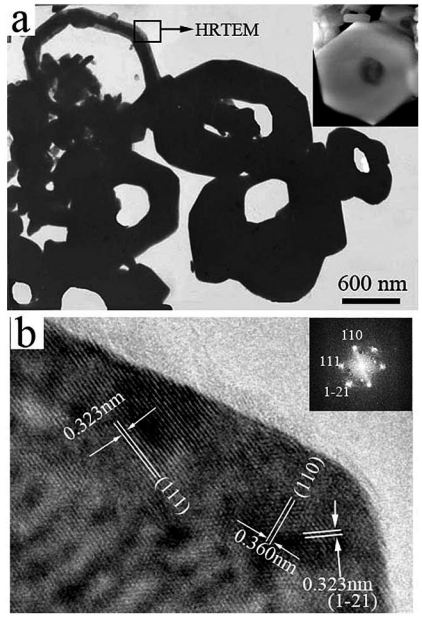

Figure 2. (a) TEM image of the obtained sample (inset: SEM image). (b) HR-TEM image obtained from the frame marked in (a) (inset: FFT pattern).

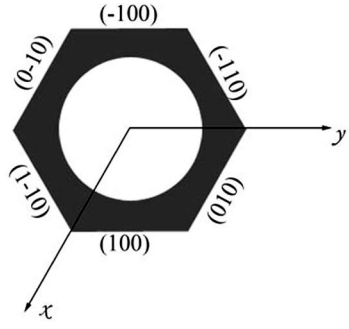

Figure 3. Schematic diagram showing a single nanoring of the as-obtained LaF_3.

Different mechanisms for the formation of ring-like structures in various synthetic systems have been reported, such as templates,[17] the Kirkendall effect,[18] the self-assembly of primary nanoparticles,[19] central-etching of disks,[20] and self-coiling of nanobelts.[4f] Based on our experiments, we believe that a central-etching of disks during crystal growth, based on the well-known Ostwald ripening process, from the inner toward the outer surface plays a key role in the formation of our LaF_3 nanorings since no other

templates/surfactants are present in the system. However, it is well known that the edges of a crystal are less stable than the center as the edges possess higher energy, therefore it was not initially clear why etching occurs at the center of the disks rather than at the edges to form the ring structures.

To investigate the driving force behind the formation of these ring-like structures in molten salt solution, we decided to monitor the reaction progress by performing time-dependent experiments. Although we are aware that the reaction does not stop immediately after the crucible is removed from the heater owing to heat-transfer reasons, we believe that the products formed at that time represent certain stages in the formation process. The TEM images obtained for these time-dependent experiments are shown in Figure 4, which shows the morphological evolution of the resulting LaF_3 nanorings. Figure 4 (a) shows the TEM image of the product obtained from the reaction after 10 min. It can clearly be seen that the morphology of most nanocrystals is that of an asymmetric near-hexagonal plate with the size of around 800 nm. The SAED pattern (Figure 4, d) of one of these crystals indicates its single-crystalline nature with an axis of [001]. On the basis of the SAED pattern, the side surfaces should be prismatic {–110} or {100} planes of hexagonal LaF_3, which are the same as those in the final LaF_3 nanoring. Furthermore, the XRD pattern (Figure S2 in the Supporting Information) also illustrates that LaF_3 nanocrystals are already well crystallized after only 10 min of reaction. Moreover, it can clearly be seen from Figure 4 (a) that there are many cavities, with a diameter of about 5 nm, on the top/bottom surfaces of the obtained plates. It can therefore be concluded that these LaF_3 nanoplates with cavities crystallize rapidly under these reaction conditions. Similar structures have also been observed by Cheng et al. from a reaction in aqueous solution.[21] The exact mechanism of cavity formation remains unclear, although we propose that their formation may be related to the growth habit and speed of crystallization.

As the reaction continues conventional Ostwald ripening occurs. Figure 4 (b) shows a TEM image of the product obtained after 1 h, which clearly shows that the centers of nanoplates are gradually disappearing and ring-like structures are forming. We suggest that the cavities in the nanoplates increase the surface area to volume ratio of the top/bottom surfaces of the nanoplates, thereby increasing their energy. As a result, the centers of nanoplates with cavities become less stable than their edges, which is why etching occurs at the center of these nanoplates rather than at their edges. In addition, molten salt syntheses are strongly influenced by the surface and interface energies between the constituents and the salts due to their strong polarity and high surface tension, thus making the etching stronger in this case. The molten salts themselves could therefore also provide an additional driving force for formation of the ring-like structures. Figure 4 (c) shows a TEM image of the sample obtained from the reaction after 3 h. It can clearly be seen that the cavities in the plate have grown so large as to almost form one big hole with only a few fragments

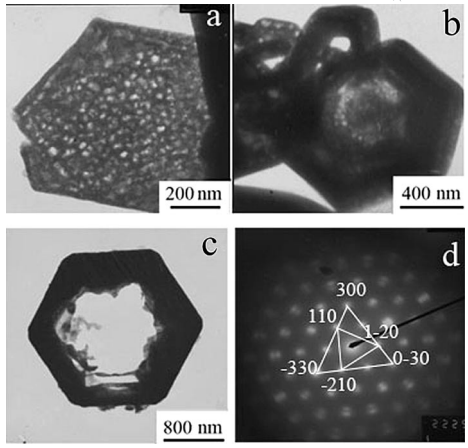

Figure 4. TEM images of products obtained from the reaction for 10 min (a), 1 h (b), and 3 h (c), and the SAED pattern (d) corresponding to the crystal in image (a).

attached. In this regard, the etching mechanism is also a dissolution-recrystallization process, with dissolution of the inner and growth of the outer surface of the plates. However, this growth is not discernible due to the variety of outer diameters of the product.

The LaF_3 ring-formation process can therefore be described as shown schematically in Figure 5. Dissolution of $La(NO_3)_3$ in the hot molten salts leads to its dissociation into La^{3+} and NO_3^- ions, and La^{3+} tends to react with F^- rapidly to give LaF_3 nuclei. Due to their high surface energy, these nuclei aggregate rapidly, probably driven by the oriented attachment process during the growth process, to form plates with many cavities in their upper/lower surfaces. The plates are then etched by the intensely polar reaction medium from these cavities outwards. Eventually, the cavities in one plate grow until they form one big hole. The etching is not uniform from plate to plate, or even within a single plate, which is why the large holes appear irregular.

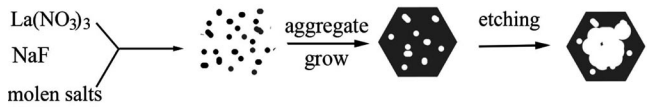

Figure 5. Schematic illustration showing the formation process for the LaF_3 nanorings.

LaF_3 has been considered to be an ideal host lattice for optically active lanthanide ions for use in luminescent applications, although different doping modes can lead to quite different emission behaviors. To study the luminescence of our as-obtained LaF_3 nanorings, products doped with 15 mol-% Eu^{3+} were prepared by the same synthetic pathway to investigate their optical properties in detail. It should be noted that this doping process alters neither the crystal structures nor the shapes of the host materials. Figure 6 shows the emission spectra for bulk LaF_3:Eu (15 mol-%), approx. 50-nm nanoparticles, and nanorings at room temperature excited at a wavelength of 395 nm. Characteris-

tic emission peaks of the $^5D_0 \rightarrow {}^7F_J$ transitions (J = 0, 1, 2, 3, 4) of the Eu^{3+} ion can clearly be seen. Monitoring the intensity of the peaks at around 590 nm due to the $^5D_0 \rightarrow {}^7F_1$ transition (Figure 6) showed that the LaF_3:Eu nanorings emit the highest fluorescence intensity among the three samples. This may be due to fluorescent quenching in bulk LaF_3:Eu^{3+} (15 mol-%) as a lower quenching concentration has been reported for a doping level of 3 mol-%.[22] At the same time, an increase in nonradiative transitions caused by surface defects as the particle size decreases means that the emission intensity of the nanorings is much higher than that of the 50-nm nanoparticles.[23]

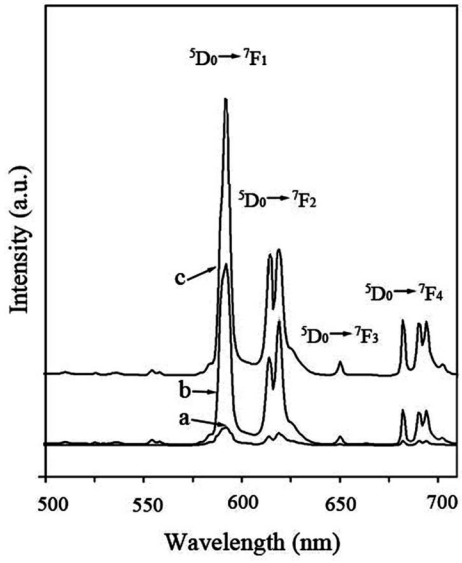

Figure 6. Room-temperature fluorescence emission spectra of LaF_3 with Eu^{3+} doping for (a) bulk, (b) 50-nm nanoparticles, and (c) nanorings (λ = 395 nm).

The relative intensity ratio of the $^5D_0 \rightarrow {}^7F_2$ and $^5D_0 \rightarrow {}^7F_1$ transitions (I_{610}/I_{590}) was calculated to be 0.763 and 0.895 for the nanorings and nanoparticles, respectively. It is well-known that the $^5D_0 \rightarrow {}^7F_2$ (ca. 610 nm) transition is an allowed electric-dipole transition and that its intensity is significantly affected by the symmetry of the local environment around the Eu^{3+} ions. The $^5D_0 \rightarrow {}^7F_1$ transition (ca. 590 nm), on the other hand, is magnetic-dipole allowed and it is relatively insensitive to the local environment around Eu^{3+}. The I_{610}/I_{590} ration could therefore be used as an indicator of the symmetry variation around the Eu^{3+} species in the host lattice, with an increase indicating an increase in the asymmetry of the coordination polyhedron around Eu^{3+} in the lattice. Furthermore, the Eu^{3+} ions at the surface are subjected to a less symmetric environment than those in the inner part of the crystals, therefore the relatively lower surface area to volume ratio of the as-prepared Eu^{3+}-doped LaF_3 nanorings compared to the 50-nm nanoparticles leads to a decrease in the $^5D_0 \rightarrow {}^7F_2$ transition.

Conclusions

In summary, we have developed a simple one-pot molten salt route for the preparation of high-quality LaF_3 nanorings in which $NaNO_3$ and KNO_3 (2:1 molar ratio) act as the reaction medium and the rare-earth nitrate and NaF the precursor. The reaction mechanism and crystal growth have been investigated, and a possible formation process for ring-like LaF_3 nanostructures proposed and discussed in detail. Furthermore, Eu^{3+}-doped LaF_3 nanorings show characteristic emission lines (500–700 nm) corresponding to transitions from $^5D_0$ to ^7F_J, with the $^5D_0 \rightarrow {}^7F_1$ red emission being the most prominent group. These results not only enrich the field of lanthanide fluoride chemistry but also allow us to study the growth and formation mechanism of nano-/microcrystals in molten salts.

Experimental Section

Preparation of LaF_3 Nanostructures and Eu^{3+}-Doped LaF_3: $NaNO_3$, KNO_3, and NaF were purchased from Tianjin Chemical Reagent Company. $La(NO_3)_3 \cdot 6H_2O$ and Eu_2O_3 were purchased from Shanghai Chemical Reagent Company. All chemicals were analytical grade and were used without further purification. In a typical synthesis, 6.7 g of molten salt (mixture of $NaNO_3$ and KNO_3; molar ratio: 1:2) was heated to 480 °C in a crucible in muffle furnace until it melted to a transparent liquid. $La(NO_3)_3 \cdot 6H_2O$ (0.001 mol) and NaF (0.003 mol) were mixed in an agate mortar in the appropriate stoichiometric ratio and ground for 10 min. This mixture was subsequently dissolved in the molten salt and maintained at 350 °C for 1.0 h. After reacting for 4 h and then cooling to room temperature, the product was obtained by washing the melt several times with deionized water to remove the nitrates, and dried at 100 °C in air for 12 h. The Eu^{3+}-doped LaF_3 nanorings were prepared in a similar manner but with 15 mol-% of the $La(NO_3)_3 \cdot 6H_2O$ precursor replaced by $Eu(NO_3)_3 \cdot 6H_2O$. The bulk LaF_3/Eu^{3+} (15 mol-%) materials were synthesized by solid synthesis by calcining stoichiometric amounts of $La(NO_3)_3 \cdot 6H_2O$, $Eu(NO_3)_3 \cdot 6H_2O$, and NaF at 700 °C for 5 h. The approximately 50-nm Eu^{3+}-doped LaF_3 nanoparticles were prepared according to a literature procedure.[24]

Characterization: The X-ray diffraction (XRD) patterns of the samples were collected using a Rigaku D/Max 2200PC diffractometer equipped with a Cu-K_α radiation source (λ = 1.5418 Å) and a graphite monochromator from 20 to 70° at a scan rate of 5.0° min^{-1}. Unit cell dimensions were determined with the JADE 5 program for X-ray diffraction pattern processing, identification, and quantification. The chemical composition of the as-prepared nanoplates, which were boiled in distilled water and then dissolved in HNO_3, was determined by ICP-MS (Agilent 7500C). The size and morphology of the products were determined by TEM (JEM100-CX), selected-area electron diffraction (SAED), and field-emission scanning electron microscopy (FE-SEM; JEOL JSM 6700F) equipped with an energy dispersive X-ray (EDX, Oxford) spectrum. HR-TEM (JEOL-2010) was used to study the intrinsic crystallography of the obtained samples. The fluorescence properties of all samples were investigated with an Edinburgh FLS920 fluorescence spectrometer equipped with a 450-W Xe lamp. The samples for fluorescence testing were prepared by dispersing the obtained nanoplates in ethanol to form approximately 0.1 wt.-% clear solutions. The asymmetric ratio was calculated by taking the ratio of the area under the peaks corresponding to the $^5D_0 \rightarrow {}^7F_2$ and $^5D_0 \rightarrow {}^7F_1$ transitions.[25]

Supporting Information (see footnote on the first page of this article): EDX image of the product and XRD pattern of the product obtained from the reaction after 10 min.

[1] a) R. Martel, H. R. Shea, P. Avouris, *Nature* **1999**, *398*, 299–299; b) M. Sano, A. Kamino, J. Okamura, S. Shinkai, *Science* **2001**, *293*, 1299–1301; c) X. Y. Kong, Y. Ding, R. Yang, Z. L. Wang, *Science* **2004**, *303*, 1348–1351; d) Y. Sun, Y. Xia, *Adv. Mater.* **2003**, *15*, 695–699; e) Q. Guo, S. J. Kim, W. N. Shafarman, R. W. Birkmire, E. A. Stach, R. Agrawal, H. W. Hillhouse, *Nano Lett.* **2008**, *8*, 2982–2987.

[2] a) J. Aizpurua, P. Hanarp, D. S. Sutherland, M. Kall, G. W. Bryant, F. J. G. de Abajo, *Phys. Rev. Lett.* **2003**, *90*, 57401–57404; b) E. M. Larssonk, J. Alegret, M. Kall, D. S. Sutherland, *Nano Lett.* **2007**, *7*, 1256–1263.

[3] a) K. L. Hobbs, P. R. Larson, G. D. Lian, J. C. Keay, M. B. Johnson, *Nano Lett.* **2004**, *4*, 167–171; b) U. Welp, V. K. Vlasko-Vlasov, G. W. Crabtree, J. Hiller, N. Zaluzec, V. Metlushko, B. Ilic, *J. Appl. Phys.* **2003**, *93*, 7056–7058; c) M. Steiner, J. Nitta, *Appl. Phys. Lett.* **2004**, *84*, 939–941; d) F. Q. Zhu, D. L. Fan, X. C. Zhu, J. G. Zhu, R. C. Cammarata, C. L. Chien, *Adv. Mater.* **2004**, *16*, 2155–2159; e) F. Yan, W. A. Goedel, *Nano Lett.* **2004**, *4*, 1193–1196; f) H. Xu, W. A. Goedel, *Angew. Chem. Int. Ed.* **2003**, *42*, 4696–4700; g) Y. D. Wang, K. Yu. Zang, S. J. Chua, M. S. Sander, S. Tripathy, C. G. Fonstad, *J. Phys. Chem. B* **2006**, *110*, 11081–11087; h) F. Q. Sun, J. C. Yu, X. C. Wang, *Chem. Mater.* **2006**, *18*, 3774–3779; i) S. Zhao, H. Roberge, A. Yelon, T. Veres, *J. Am. Chem. Soc.* **2006**, *128*, 12352–12353; j) S. Wang, G. J. Yu, J. L. Gong, Q. T. Li, H. J. Xu, D. Z. Zhu, Z. Y. Zhu, *Nanotechnology* **2006**, *17*, 1584–1598.

[4] a) B. Liu, H. C. Zeng, *J. Am. Chem. Soc.* **2005**, *127*, 18262–18268; b) F. Li, Y. Ding, P. X. X. Gao, X. Q. Xin, Z. L. Wang, *Angew. Chem. Int. Ed.* **2004**, *43*, 5238–5242; c) Y. Peng, A. W. Xu, B. Deng, M. Antonietti, H. Cölfen, *J. Phys. Chem. B* **2006**, *110*, 2988–2993; d) L. P. Jiang, S. Xu, J. M. Zhu, J. R. Zhang, J. J. Zhu, H. Y. Chen, *Inorg. Chem.* **2004**, *43*, 5877–5883; e) J. J. Miao, R. L. Fu, J. M. Zhu, K. Xu, J. J. Zhu, H. Y. Chen, *Chem. Commun.* **2006**, 3013–3015; f) G. Z. Shen, D. Chen, *J. Am. Chem. Soc.* **2006**, *128*, 11762–11763; g) C. Jia, L. Sun, F. Luo, X. Han, *J. Am. Chem. Soc.* **2008**, *130*, 16968–16977; h) X. Hu, J. C. Yu, J. Gong, Q. Li, G. Li, *Adv. Mater.* **2007**, *19*, 2324–2329.

[5] T. A. O'Donnell, *Eur. J. Inorg. Chem.* **2001**, 21–34.

[6] a) H. Chen, C. P. Grey, *Adv. Mater.* **2008**, *20*, 2206–2210; b) C.-Y. Xu, L. Zhen, R. Yang, Z. L. Wang, *J. Am. Chem. Soc.* **2007**, *129*, 15444–15445; c) J. Chen, X. Xing, A. Waston, W. Wang, R. Yu, J. Deng, L. Yan, C. Sun, X. Chen, *Chem. Mater.* **2007**, *19*, 3598–3600; d) Y. Mao, T.-J. Park, F. Zhang, H. Zhou, S. S. Wong, *Small* **2007**, *3*, 1122–1139; e) H. Liu, C. Hu, Z. Wang, *Nano Lett.* **2006**, *6*, 1535–1540; f) X. Wang, J. Zhuang, Y. Li, *Eur. J. Inorg. Chem.* **2004**, 946–948.

[7] B. Cui, H. Lin, J. Li, X. Li, J. Yang, J. Tao, *Adv. Funct. Mater.* **2008**, *18*, 1440–1447.

[8] a) K. Kömpe, H. Borchert, J. Storz, A. Lobo, S. Adam, T. Möller, M. Haase, *Angew. Chem. Int. Ed.* **2003**, *42*, 5513–5516; b) J. W. Stouwdam, G. A. Hebbink, J. Huskens, F. C. J. M. van Veggel, *Chem. Mater.* **2003**, *15*, 4604–4616; c) S. Heer, O. Lehmann, M. Haase, H. Güdel, *Angew. Chem. Int. Ed.* **2003**, *42*, 3179–3182; d) F. Meiser, C. Cortez, F. Caruso, *Angew. Chem. Int. Ed.* **2004**, *43*, 5954–5957.

[9] Y. W. Zhang, X. Sun, R. Si, L. P. You, C. H. Yan, *J. Am. Chem. Soc.* **2005**, *127*, 3260–3261.

[10] a) X. Wang, Y. Li, *Angew. Chem. Int. Ed.* **2003**, *42*, 3497–3500; b) X. Wang, Y. Li, *Chem. Eur. J.* **2003**, *9*, 5627–5635; c) R. Yan, Y. Li, *Adv. Funct. Mater.* **2005**, *15*, 763–770; d) X. Wang, J. Zhuang, Q. Peng, Y. Li, *Inorg. Chem.* **2006**, *45*, 6661–6665.

[11] L. Zhu, Q. Li, X. Liu, J. Li, Y. Zhang, J. Meng, X. Cao, *J. Phys. Chem. C* **2007**, *111*, 5898–5903.

[12] M. Wang, Q. L. Huang, H. X. Zhou, X. T. Chen, Z. L. Xue, X. Z. You, *Cryst. Growth Des.* **2007**, *7*, 2106–2111.

[13] J.-L. Lemyre, A. M. Ritcey, *Chem. Mater.* **2005**, *17*, 3040–3043.

[14] F. Tao, Z. Wang, L. Yao, W. Cai, X. Li, *J. Phys. Chem. C* **2007**, *111*, 3241–3245.

[15] C. Li, J. Yang, P. Yang, H. Lian, J. Lin, *Chem. Mater.* **2008**, *20*, 4317–4326.

[16] a) L. Zhu, X. Liu, J. Meng, X. Cao, *Cryst. Growth Des.* **2007**, *7*, 2505–2511; b) M. Wang, Q. Huang, J. Hong, X. Chen, Z. Xue, *Cryst. Growth Des.* **2006**, *6*, 1972–1974; c) M. Wang, Q. Huang, J. Hong, X. Chen, Z. Xue, *Cryst. Growth Des.* **2006**, *6*, 2169–2173.

[17] a) Y. Sun, Y. Xia, *Adv. Mater.* **2003**, *15*, 695–699; b) G. S. Metraux, Y. C. Cao, R. Jin, C. A. Mirkin, *Nano Lett.* **2003**, *3*, 519–522.

[18] C. Peng, L. Gao, S. Yang, *Chem. Commun.* **2007**, 4372–4374.

[19] Z. Liu, R. Levicky, *Nanotechnology* **2004**, *15*, 1483–1488.

[20] J.-J. Miao, R.-L. Fu, J.-M. Zhu, K. Xu, J.-J. Zhu, H.-Y. Chen, *Chem. Commun.* **2006**, 3013–3015.

[21] Y. Cheng, Y. Wang, Y. Zheng, Y. Qin, *J. Phys. Chem. B* **2005**, *109*, 11548–11551.

[22] J.-X. Meng, M.-F. Zhang, Y.-L. Liu, S.-Q. Man, *Spectrochim. Acta Part A* **2007**, *66*, 81–85.

[23] B. M. Tissue, *Chem. Mater.* **1998**, *10*, 2837–2845.

[24] Y. Tian, X. Jiao, J. Zhang, N. Sui, D. Chen, G. Hong, *J. Nanopart. Res.*, DOI: 10.110/s11051-009-9590-5.

[25] V. Sudarsan, F. C. J. M. van Veggel, R. A. Herring, M. Raudsepp, *J. Mater. Chem.* **2005**, *15*, 1332–1342.

Received: February 5, 2009
Published Online: April 23, 2009

